

# Landau model for the elastic properties of the ferroelastic crystal $\text{Rb}_4\text{LiH}_3(\text{SO}_4)_4$

G Quirion<sup>1</sup>, W Wu<sup>2</sup>, O Aktas<sup>1</sup>, J Rideout<sup>1</sup>, M J Clouter<sup>1</sup> and B Mróz<sup>3</sup>

<sup>1</sup> Department of Physics and Physical Oceanography, Memorial University, St John's, Newfoundland, A1B 3X7, Canada

<sup>2</sup> Department of Physics, University of Toronto, Toronto, ON, Canada

<sup>3</sup> Faculty of Physics, Adam Mickiewicz University, Poznan, Poland

Received 8 June 2009, in final form 7 October 2009

Published 21 October 2009

Online at [stacks.iop.org/JPhysCM/21/455901](http://stacks.iop.org/JPhysCM/21/455901)

## Abstract

Using sound velocity measurements, we report a detailed investigation of the elastic properties of  $\text{Rb}_4\text{LiH}_3(\text{SO}_4)_4$  realized as a function of temperature and pressure. Results are compared to predictions of a phenomenological Landau model. Supported by recent Raman scattering measurements, we assume that the  $4 \rightarrow 2$  structural transformation observed at  $T_c = 134$  K corresponds to a pseudo-proper ferroelastic transition. For the numerical analysis, all coupling parameters are determined using the temperature dependence of the frequency of the soft optical B mode, the temperature dependence of spontaneous strains, and the pressure dependence  $dT_c/dP = 191 \pm 2$  K GPa<sup>-1</sup> also determined in this work. Our comparison indicates that the  $4 \rightarrow 2$  structural transition in  $\text{Rb}_4\text{LiH}_3(\text{SO}_4)_4$  is fully consistent with predictions derived using our pseudo-proper ferroelastic model. Thus, all data presented in this paper corroborate that the mechanism leading to the structural transition at  $T_c = 134$  K results from the softening of the B optical mode observed at  $31$  cm<sup>-1</sup>. This detailed analysis also refutes the idea that  $\text{Rb}_4\text{LiH}_3(\text{SO}_4)_4$  shows incomplete softening of the soft acoustic mode also associated with that structural transition.

(Some figures in this article are in colour only in the electronic version)

## 1. Introduction

Over the years, there have been many controversies regarding the properties of the ferroelastic compound  $\text{Rb}_4\text{LiH}_3(\text{SO}_4)_4$ . Initially designated as  $\text{LiRb}_5(\text{SO}_4)_3 \cdot 1.5\text{H}_2\text{SO}_4$  [1–4], subsequent chemical analysis revealed that  $\text{Rb}_4\text{LiH}_3(\text{SO}_4)_4$  is the proper chemical formulation. The room temperature point group assignment for  $\text{Rb}_4\text{LiH}_3(\text{SO}_4)_4$  [5, 6] was also incorrect. This led to the misleading interpretation that the structural transformation at 134 K was a  $4mm \rightarrow 2mm$  ferroelastic phase transition. It was only after additional x-ray [7] and neutron diffraction [8] measurements that the correct  $4 \rightarrow 2$  group-subgroup symmetry change was identified. Subsequently, the elastic properties of  $\text{Rb}_4\text{LiH}_3(\text{SO}_4)_4$  have been revisited by different groups. Both experimental approaches, Brillouin scattering [9] and ultrasonic study [10], have now confirmed that the effective elastic constant  $(C_{11} - C_{12})/2$  partially softens as the temperature is decreased down to  $T_c$ . Nonetheless, in order to account for their respective findings, different models have been used. On the one hand, the ultrasonic velocity

measurements [10] are interpreted within the framework of a pseudo-proper ferroelastic model driven by an order parameter  $Q$  which differs from the strains. On the other hand, Mróz *et al* [9] analyzed their data using a proper ferroelastic model assuming that the strain combination  $e_s = \alpha_1(e_1 - e_2) + \alpha_6 e_6$  is the order parameter. In their interpretation they also claimed that the softening of the acoustic mode, associated with the spontaneous strain  $e_s$ , is incomplete at  $T_c$ . This conclusion is atypical as all known proper [11] and pseudo-proper [12, 13] ferroelastic compounds show complete softening for a continuous phase transition. For a general review on proper and pseudo-proper ferroelastic phase transitions, readers are invited to consult papers by Carpenter *et al* [14] and Salje [15].

In order to elucidate the nature of the ferroelastic transition, as well as to validate or refute the possibility of incomplete softening in  $\text{Rb}_4\text{LiH}_3(\text{SO}_4)_4$ , we present a detailed investigation of the elastic properties measured as a function of temperature and pressure. These results are complemented by new Raman measurements [16] which

indicate that the character of the ferroelastic transition observed at  $T_c = 134$  K is more likely pseudo-proper. Thus, our ultrasonic velocity data are compared to numerical predictions derived using a Landau model. As we show, the pseudo-proper ferroelastic model accounts very well for the temperature/pressure dependence of the elastic moduli, the temperature dependence of the spontaneous strains, the temperature dependence of the soft optical mode [16], and the pressure dependence of  $T_c$ . Finally, our analysis also indicates that the elastic properties of  $\text{Rb}_4\text{LiH}_3(\text{SO}_4)_4$  are compatible with complete softening of the acoustic mode at  $T_c$ .

The remainder of the paper is organized as follows. In section 2 we briefly describe the experimental methods used for this investigation, while section 3 provides the theoretical background related to a pseudo-proper ferroelastic phase transition. Section 4 is dedicated to the determination of all coupling coefficients. This is achieved principally using the pressure dependence of  $T_c$ , the spontaneous strains, and the temperature dependence of the soft optical mode. In section 5, the elastic moduli determined from ultrasonic velocity data are compared to the model's predictions. Section 6 is devoted to the analysis of the temperature dependence of the soft acoustic mode. We specifically compare the soft mode effective modulus with predictions obtained from the pseudo-proper model. This comparison shows how velocity measurements, obtained over a wide temperature range, could in principle be used to determine the nature of ferroelastic transitions. Finally, a summary of the principal findings is presented in section 7.

## 2. Experiment

The  $\text{Rb}_4\text{LiH}_3(\text{SO}_4)_4$  crystal was grown by the Crystal Physics Laboratory of the Faculty of Physics at Mickiewicz University, Poland [9]. For this investigation, several samples in the form of about  $3 \times 3 \times 3$  mm<sup>3</sup> cubes were used to measure the sound velocity along different crystallographic directions. Longitudinal and transverse waves were generated and detected using 30 MHz lithium niobate transducers mounted on one of the parallel faces of the crystal. The relative variation in the sound velocity ( $\Delta V/V$ ) with a resolution of 1 ppm was measured as a function of temperature and pressure using a pulsed acoustic interferometer. For measurements under pressure, the transducer-sample assemblage was inserted in a Cu–Be pressure cell filled with a 3-methyl-1-butanol fluid acting as the pressure-transmitting medium. A small wire of lead mounted close to the sample was used to determine the actual pressure at different temperatures [17].

## 3. Pseudo-proper ferroelastic model

According to the classification adopted by Toledano *et al* [18], a pseudo-proper ferroelastic transition is not strictly speaking a strain-induced structural transformation. However, one of the necessary requirements is that the primary order parameter  $Q$  must belong to the same irreducible representation [18, 14] as that of the spontaneous strain  $e_s$ , acting as a secondary order parameter. Under this condition, the invariant bilinear

coupling term  $Qe_s$  leads to softening of the acoustic mode associated with  $e_s$ . Thus, the observation of soft acoustic and optical modes, both with the same representation, generally leaves no doubt regarding the nature of the ferroelastic transition. For example, it has been clearly established that the elastic instability in ferroelastic compounds  $\text{BiVO}_4$  [12],  $\text{LaP}_5\text{O}_{14}$  [19], and  $\text{SnO}_2$  [13] is triggered by the softening of an optical mode. In the case of  $\text{Rb}_4\text{LiH}_3(\text{SO}_4)_4$ , according to group theory [20], a  $4 \rightarrow 2$  pseudo-proper ferroelastic transition could be driven by the softening of a B optical mode which couples to the strain  $e_s = \alpha_1(e_1 - e_2) + \alpha_6 e_6$  [18]. As softening of the B active Raman mode [16] and acoustic mode (this paper) have been confirmed, it is sensible to assume that the structural transition in  $\text{Rb}_4\text{LiH}_3(\text{SO}_4)_4$  is pseudo-proper ferroelastic. Thus, in this section we present a Landau free energy that can be used to predict the behavior of the soft optical mode, the spontaneous strains, and the temperature/pressure dependence of the elastic moduli. The total Gibbs energy considered here is similar to the one derived by David [21] to account for the  $4/m \rightarrow 2/m$  ferroelastic transition observed in  $\text{BiVO}_4$ . As the  $4 \rightarrow 2$  ferroelastic transition belongs to the same irreducible representation, we adopt the same phenomenological approach for  $\text{Rb}_4\text{LiH}_3(\text{SO}_4)_4$ .

For convenience, we divide the Landau expansion of the Gibbs free energy into four distinct contributions

$$G(Q, e_\alpha) = F_L(Q) + F_{\text{el}}(e_\alpha) + F_c(Q, e_\alpha) + F_P(P, e_\alpha) \quad (1)$$

where  $F_L(Q)$  is the usual second-order Landau free energy expanded in terms of an order parameter  $Q$ ,

$$F_L(Q) = \frac{1}{2}A Q^2 + \frac{1}{4}A_4 Q^4. \quad (2)$$

As shown in [22], the saturation of the order parameter in ferroelastic compounds can be accounted for by using

$$A = \alpha \theta_s \left[ \coth\left(\frac{\theta_s}{T}\right) - \coth\left(\frac{\theta_s}{T_o}\right) \right], \quad (3)$$

which is equivalent to the usual Landau term  $A = \alpha(T - T_o)$  in the high temperature limit ( $T \gg \theta_s$ ). The elastic energy  $F_{\text{el}}(e_\alpha)$  for the high temperature point group 4 symmetry [23] is

$$\begin{aligned} F_{\text{el}}(e_\alpha) = & \frac{1}{2}C_{11}(e_1^2 + e_2^2) + \frac{1}{2}C_{33}e_3^2 + \frac{1}{2}C_{44}(e_4^2 + e_5^2) \\ & + \frac{1}{2}C_{66}e_6^2 + C_{12}e_1e_2 + C_{13}(e_1 + e_2)e_3 \\ & + C_{16}(e_1 - e_2)e_6 \end{aligned} \quad (4)$$

where  $C_{\alpha\beta}$  represent the bare elastic constants of the high temperature phase. Here, the elastic constants  $C_{\alpha\beta}$  and strains  $e_\alpha$  are defined relative to the Voigt notation ( $\alpha, \beta = 1 \dots 6$ ). The coupling energy  $F_c(Q, e_\alpha)$ , representing the coupling between the strain components  $e_\alpha$  and the order parameter  $Q$ , can be obtained using simple symmetry arguments [21]. Thus, the lower-order invariant coupling terms correspond to

$$\begin{aligned} F_c(Q, e_\alpha) = & \beta Q(e_1 - e_2) + \gamma Q e_6 + \delta Q^2 e_3 + \lambda Q^2(e_1 + e_2) \\ & + \zeta e_4 e_5 Q + \eta(e_4^2 - e_5^2) Q. \end{aligned} \quad (5)$$

**Table 1.** Values of the bare elastic constants.

Bare elastic constant	$10^{10}$ (N m <sup>-2</sup> )
$C_{11}^o$	5.67
$C_{12}^o$	0.50
$C_{13}^o$	1.80
$C_{16}^o$	-0.24
$C_{33}^o$	5.14
$C_{44}^o$	0.74
$C_{66}^o$	1.14

Finally, in order to calculate the pressure dependence of the elastic constants, we also consider the hydrostatic pressure contribution

$$F_P(P, e_\alpha) = P(e_1 + e_2 + e_3). \quad (6)$$

Using the equilibrium condition,  $\partial G/\partial e_\alpha = 0$ , solutions for the spontaneous strains  $e_\alpha(Q, P)$  are obtained and correspond to

$$\begin{aligned} e_1 - e_2 &= \frac{2(\gamma C_{16} - \beta C_{66})}{C_d} Q \\ e_1 + e_2 &= \frac{2(\delta C_{13} - \lambda C_{33})}{C_a} Q^2 - \frac{2(C_{33} - C_{13})}{C_a} P \\ e_3 &= -\frac{\delta(C_{11} + C_{12}) - 2\lambda C_{13}}{C_a} Q^2 - \frac{C_g}{C_a} P \\ e_4 = 0 \quad e_5 = 0 \quad e_6 &= -\frac{\gamma(C_{11} - C_{12}) - 2\beta C_{16}}{C_d} Q \end{aligned} \quad (7)$$

with

$$\begin{aligned} C_a &= (C_{11} + C_{12})C_{33} - 2C_{13}^2 \\ C_d &= (C_{11} - C_{12})C_{66} - 2C_{16}^2 \\ C_g &= C_{11} + C_{12} - 2C_{13}. \end{aligned} \quad (8)$$

Subsequently, solutions for the order parameter  $Q(T, P)$ , the critical temperature  $T_c$  and  $dT_c/dP$  are obtained from the minimization of the free energy with respect to  $Q$ . These solutions can be expressed as

$$Q^2(T, P) = \frac{\alpha C_a}{\Delta} \left\{ \theta_s \left[ \coth\left(\frac{\theta_s}{T_c}\right) - \coth\left(\frac{\theta_s}{T}\right) \right] + \frac{dT_c}{dP} P \right\} \quad (9)$$

$$\frac{C_b}{\alpha C_d} = \theta_s \left[ \coth\left(\frac{\theta_s}{T_c}\right) - \coth\left(\frac{\theta_s}{T_o}\right) \right] \quad (10)$$

$$\frac{dT_c}{dP} = 2 \frac{C_c}{\alpha C_a} \quad (11)$$

where

$$\begin{aligned} C_b &= \gamma^2(C_{11} - C_{12}) + 2\beta(\beta C_{66} - 2\gamma C_{16}) \\ C_c &= \delta(C_{11} + C_{12} - 2C_{13}) + 2\lambda(C_{33} - C_{13}) \end{aligned} \quad (12)$$

$$\Delta = A_4 C_a - 4\lambda^2 C_{33} - 2(C_{11} + C_{12})\delta^2 + 8\delta\lambda C_{13}.$$

Due to the bilinear coupling terms  $\beta Q(e_1 - e_2) + \gamma Q e_6$ , the transition temperature  $T_c$ , given by equation (10), is shifted with respect to the uncoupled limit  $T_o$ .

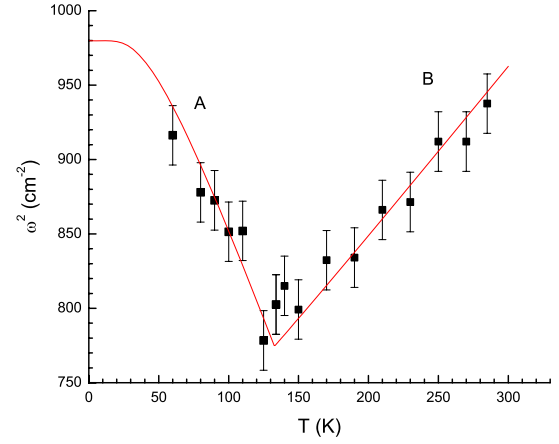


**Figure 1.** Temperature dependence of the frequency squared of the B/A active Raman modes. Symbols correspond to data published by Aktas *et al* [16] while continuous lines correspond to predictions using equation (14).

#### 4. Determination of the coupling coefficients

As mentioned previously, recent Raman measurements [16] indicate that the character of the ferroelastic transition in  $\text{Rb}_4\text{LiH}_3(\text{SO}_4)_4$  is pseudo-proper. In this case, the order parameter  $Q$  can be associated with the normal coordinate vibrations of a soft mode. If one treats this mode as a simple harmonic oscillator, the first term of equation (2) can be directly written as

$$\frac{1}{2} m \omega_Q^2(T) Q^2 = \frac{1}{2} A Q^2, \quad (13)$$

where, according to group theory [20],  $\omega_Q$  must correspond to the frequency of a B mode for a  $4 \rightarrow 2$  pseudo-proper ferroelastic transition. Using the total free energy, the temperature dependence of  $\omega_Q^2(T) = \partial^2 G/\partial Q^2$  [13] corresponds to

$$\begin{aligned} m \omega_Q^2(T) &= \alpha \theta_s \left[ \coth\left(\frac{\theta_s}{T}\right) - \coth\left(\frac{\theta_s}{T_o}\right) \right] \simeq \alpha(T - T_o) \\ T &> T_c, \\ m \omega_Q^2(T) &= -2 \frac{C_a A_4}{\Delta} \alpha \theta_s \left[ \coth\left(\frac{\theta_s}{T}\right) - \coth\left(\frac{\theta_s}{T_c}\right) \right] + \frac{C_b}{C_d} \\ T &< T_c. \end{aligned} \quad (14)$$

The Raman scattering data are very valuable as they can be used to obtain good numerical estimates for the model's parameter  $T_o$ . Using the numerical values reported in tables 1 and 2, we compare in figure 1 predictions given by equation (14) with recent Raman data [16] obtained for the low frequency B/A mode (the symmetry of the soft mode in the low temperature monoclinic phase is A). As shown, the peculiar temperature dependence of the soft mode is well accounted for using  $T_o = -510$  K and  $\theta_s = 65$  K; the saturation temperature  $\theta_s$  has been estimated from the temperature dependence of the strains (see figure 3).

For our numerical analysis, the elastic constants have been deduced from ultrasonic velocity measurements (this

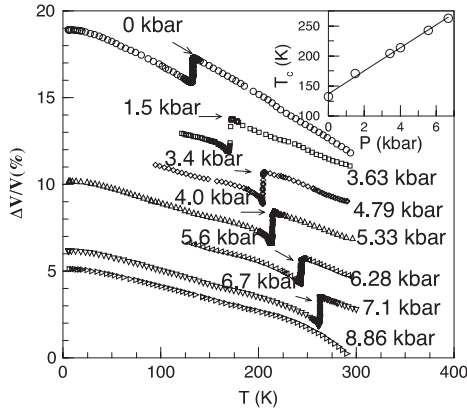


**Figure 2.** Temperature dependence of the sound velocity of longitudinal waves propagating along the  $z$ -axis obtained at different pressures. The inset shows the pressure dependence of the ferroelastic critical temperature  $T_c$  for  $\text{Rb}_4\text{LiH}_3(\text{SO}_4)_4$ .

**Table 2.** Values of the coupling constants deduced from the soft optical mode, spontaneous strains, and the pressure dependence of  $T_c$ .

Variables	Values
$\alpha$	$6.74 \times 10^9$
$\theta_s$	65
$A_4$	$1.64 \times 10^{17}$
$T_o$	-868 K
$T_c$	134 K
$\beta$	$-3.35 \times 10^{11}$
$\gamma$	$-1.14 \times 10^{10}$
$\delta$	$2.06 \times 10^{13}$
$\lambda$	$1.10 \times 10^{13}$
$\eta$	$-1.00 \times 10^{10}$
$\zeta$	$2.00 \times 10^{10}$
$\rho$	2810

work). Values reported in table 1 correspond to bare elastic constants in the absence of any coupling or anharmonic softening. For that reason, those values differ slightly from previous published data [10, 9]. In order to determine the pressure dependence of  $T_c$  (equation (11)), we also performed a series of sound velocity measurements at different pressures. These results, which show the temperature dependence of the velocity of longitudinal waves propagating along the  $z$ -axis, are presented in figure 2. This mode is particularly convenient as the ferroelastic transition temperature coincides with a sudden drop in the value of the velocity ( $\Delta V/V \sim 2\%$ ). As shown in figure 2, the ferroelastic transition temperature is very sensitive to pressure and increases at a rate of  $dT_c/dP = 191 \pm 2 \text{ K GPa}^{-1}$ .

Using the value of  $dT_c/dP$  (this work), the spontaneous strain data [8], and  $T_o$  determined from the Raman data [16], the remaining coefficients  $\gamma$ ,  $\beta$ ,  $\delta$ ,  $\lambda$ , and  $A_4$  have been obtained using

$$\frac{C_b}{\alpha C_d} = T_c - T_o = 642.8 \text{ K}$$

$$\frac{dT_c}{dP} = 2 \frac{C_c}{\alpha C_a} = 191 \text{ K GPa}^{-1}$$

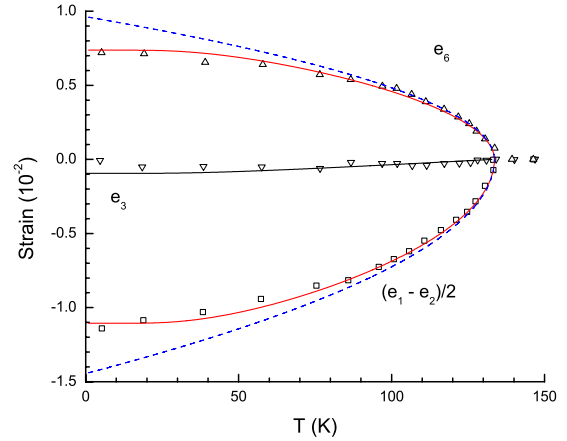


**Figure 3.** Temperature dependence of the spontaneous strains (symbols) obtained by Mróz *et al* [8]. Here the Voigt notation representations  $e_1 - e_2 = e_{11} - e_{22}$  and  $e_6 = 2e_{12}$  have been used. The continuous lines are obtained using equation (7) with the order parameter  $Q$  given by equation (9), while the broken lines correspond to mean-field predictions with  $Q \propto \sqrt{T_c - T}$ .

$$\frac{e_1 - e_2}{e_6} = -\frac{2(\gamma C_{16} - \beta C_{66})}{\gamma(C_{11} - C_{12}) - 2\beta C_{16}} = 3$$

$$e_6(0 \text{ K}) = -\frac{\gamma(C_{11} - C_{12}) - 2\beta C_{16}}{C_d} Q_o = 0.0096$$

$$e_3(0 \text{ K}) = \frac{\delta(C_{11} + C_{12}) - 2\lambda C_{13}}{C_a} Q_o^2 = -0.0016$$

$$Q_o^2 \simeq \frac{\alpha T_c}{A_4}. \quad (15)$$

The last coefficients  $\zeta$  and  $\eta$  are set by hand in order to reproduce the experimental data obtained on  $C_{44}$ . The numerical values derived from this set of equations are reported in table 2. To show the pertinence of the numerical procedure, we compare in figure 3 the calculated spontaneous strains (equation (7) with coefficients given in tables 1 and 2) to the experimental data obtained by Mróz *et al* [8]. The numerical calculations (continuous lines) using the temperature dependence of the order parameter defined in equation (9) are also compared to the usual mean-field predictions where  $Q \propto \sqrt{T_c - T}$  (broken lines). As shown, setting the saturation temperature,  $\theta_s = 65 \text{ K}$ , adequately accounts for the temperature dependence of the strains, even at low temperatures.

## 5. Elastic properties and experimental results

As all elastic and coupling constants are determined, the model can be used to calculate the temperature/pressure dependence of the elastic constants using [24]

$$C_{mn}^* = \frac{\partial^2 G}{\partial e_m \partial e_n} - \frac{\partial^2 G}{\partial Q \partial e_m} \left( \frac{\partial^2 G}{\partial Q^2} \right)^{-1} \frac{\partial^2 G}{\partial e_n \partial Q}. \quad (16)$$

As shown in table 3, all 13 independent elastic constants of the monoclinic phase are obtained, illustrating that the model

**Table 3.** Temperature/pressure dependence of the elastic constants for a  $4 \rightarrow 2$  pseudo-ferroelastic phase transition. The superscript  $o$  corresponds to bare elastic constants in the absence of coupling or anharmonic softening.

Tetragonal 4	Monoclinic 2
$C_{11} \rightarrow C_{11}^o - \frac{\beta^2}{A(T) - \alpha \frac{d\bar{\epsilon}_c}{dP}} P$	$C_{11}^o - \frac{(\beta + 2\lambda Q)^2}{A(T_c) + 2A_4 Q^2}$
$C_{22} \rightarrow C_{11}^o - \frac{\beta^2}{A(T) - \alpha \frac{d\bar{\epsilon}_c}{dP}} P$	$C_{11}^o - \frac{(\beta - 2\lambda Q)^2}{A(T_c) + 2A_4 Q^2}$
$C_{33} \rightarrow C_{33}^o$	$C_{33}^o - \frac{4\delta^2 Q^2}{A(T_c) + 2A_4 Q^2}$
$C_{44} \rightarrow C_{44}^o$	$C_{44}^o + 2\eta Q^2$
$C_{55} \rightarrow C_{44}^o$	$C_{44}^o - 2\eta Q^2$
$C_{66} \rightarrow C_{66}^o - \frac{\gamma^2}{A(T) - \alpha \frac{d\bar{\epsilon}_c}{dP}} P$	$C_{66}^o - \frac{\gamma^2}{A(T_c) + 2A_4 Q^2}$
$C_{12} \rightarrow C_{12}^o + \frac{\beta^2}{A(T) - \alpha \frac{d\bar{\epsilon}_c}{dP}} P$	$C_{12}^o + \frac{(\beta + 2\lambda Q)(\beta - 2\lambda Q)}{A(T_c) + 2A_4 Q^2}$
$C_{13} \rightarrow C_{13}^o$	$C_{13}^o - \frac{2\delta Q(\beta + 2\lambda Q)}{A(T_c) + 2A_4 Q^2}$
$C_{16} \rightarrow C_{16}^o - \frac{\beta\gamma}{A(T) - \alpha \frac{d\bar{\epsilon}_c}{dP}} P$	$C_{16}^o - \frac{\gamma(\beta + 2\lambda Q)}{Y(Q^2)}$
$C_{23} \rightarrow C_{13}^o$	$C_{13}^o + \frac{2\delta Q(\beta - 2\lambda Q)}{A(T_c) + 2A_4 Q^2}$
$C_{26} \rightarrow -C_{16}^o + \frac{\beta\gamma}{A(T) - \alpha \frac{d\bar{\epsilon}_c}{dP}} P$	$-C_{16}^o + \frac{\gamma(\beta - 2\lambda Q)}{A(T_c) + 2A_4 Q^2}$
$C_{36} \rightarrow 0$	$-\frac{2\gamma\delta Q}{A(T_c) + 2A_4 Q^2}$
$C_{45} \rightarrow 0$	$\zeta Q$

properly characterizes a  $4 \rightarrow 2$  structural change. Our calculation also indicates that, even in the high temperature phase (tetragonal),  $C_{11}$ ,  $C_{12}$ ,  $C_{16}$ , and  $C_{66}$  are re-normalized via the coupling with the soft optical B mode, leading to a nonlinear temperature/pressure dependence. These predictions can be compared to effective elastic moduli,  $\rho v^2$ , (figures 5 and 6) determined via acoustic velocity measurements. The expressions of  $\rho v^2$  as a function of the elastic constants are reported in table 4 [23]. These expressions correspond to longitudinal (L) and transverse (T) modes propagating along the principal crystallographic directions of the low temperature phase (monoclinic group).

The temperature/pressure dependence of the elastic constants listed in table 3 correspond to the contribution due to the soft optical mode alone. Before any comparison can be performed, contributions associated with all other modes need to be taken into account. As these contributions are not part of the Landau formulation, they are dealt with separately using a phenomenological approach. As shown by Varshni [25], the usual lattice contribution (often referred to as the anharmonic contribution) can be well accounted for using an empirical expression [26] such as

$$C_{\text{anh}} = C^o (1 - D \bar{\epsilon}_{\text{ph}}) \quad (17)$$

where  $C^o$  is the bare elastic constant at 0 K,  $D$  represents the coupling strength, and  $\bar{\epsilon}_{\text{ph}}$  is the mean energy per oscillator. Calculating the average phonon energy using the Einstein model and assuming a linear pressure dependence, the temperature/pressure dependence of  $C_{\text{anh}}$  can be written as

$$C_{\text{anh}} = C^o \left( 1 - \frac{\alpha_T}{e^{\Theta/T} - 1} \right) (1 + \alpha_P P). \quad (18)$$

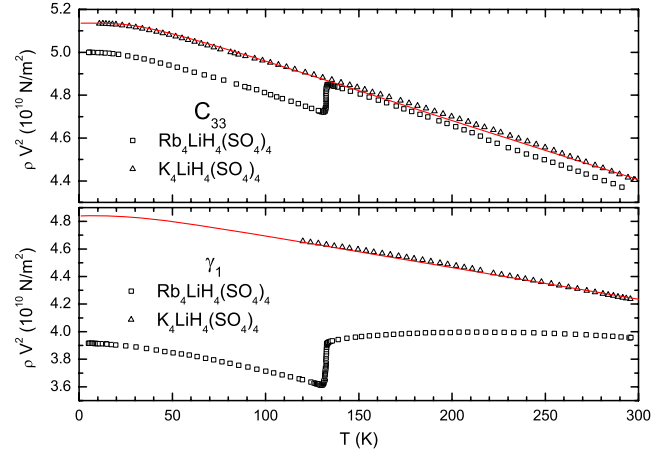


**Figure 4.** Comparison of the elastic properties of  $\text{Rb}_4\text{LiH}_3(\text{SO}_4)_4$  and the isomorphous compound  $\text{K}_4\text{LiH}_3(\text{SO}_4)_4$  using the temperature dependence of  $C_{33}$  and  $\gamma_1$ . The continuous lines represent fits obtained using equation (18) with the coefficients listed in table 5.

Fortunately, in the case of  $\text{Rb}_4\text{LiH}_3(\text{SO}_4)_4$ , the anharmonic contribution can be evaluated independently using velocity measurements for the isomorphous compound  $\text{K}_4\text{LiH}_3(\text{SO}_4)_4$ . As that compound shows no ferroelastic transition [9], the temperature dependence of the elastic properties is solely due to the anharmonic contribution, equation (18).

For that purpose, a series of sound velocity measurements have been performed on  $\text{K}_4\text{LiH}_3(\text{SO}_4)_4$  as a function of temperature/pressure. After fitting with equation (18), values for  $\Theta$ ,  $\alpha_T$ , and  $\alpha_P$  have been determined, see table 5. The set of coefficients ( $\Theta_i$ ,  $\alpha_{T_i}$ ,  $\alpha_{P_i}$ ) with  $i = 1$  are for  $C_{11}$  and  $C_{22}$  while  $i = 3$  represents the anharmonic contribution for  $C_{33}$ . The last series of coefficients,  $i = 4$ , is associated with the temperature/pressure dependence of  $C_{44}$ ,  $C_{55}$ , and  $C_{66}$ .

As an example, we present in figure 4 the fit obtained on  $\text{K}_4\text{LiH}_3(\text{SO}_4)_4$  for the effective modulus associated with longitudinal waves propagating along  $z$  and  $x$  ( $C_{33}$  and  $\gamma_1$ ). These results are also compared with equivalent measurements realized on  $\text{Rb}_4\text{LiH}_3(\text{SO}_4)_4$ . In the paraelastic phase, this comparison shows that the temperature dependence of  $C_{33}$  is practically identical in both materials. This is consistent with the model's prediction as no temperature dependence due to the soft optical mode is expected on  $C_{33}$  (see table 3 in the tetragonal phase). This indicates that the anharmonic contributions for these two isomorphous compounds are indeed very similar. Hence, the difference in the temperature dependence of  $\gamma_1$  for  $\text{K}_4\text{LiH}_3(\text{SO}_4)_4$  and  $\text{Rb}_4\text{LiH}_3(\text{SO}_4)_4$  can be attributed to coupling with the soft optical mode.

As all parameters are now determined, it is straightforward to carry out a detailed comparison between the numerical and experimental effective moduli. These comparisons as a function of temperature and pressure are presented in figures 5 and 6, respectively. Here, numerical predictions correspond to continuous lines with the experimental data represented by symbols. As shown in figures 5 and 6, the largest variation, 77%, is observed on the effective modulus  $\gamma_5$  associated with transverse waves propagating along  $[110]$  with a polarization along  $[1\bar{1}0]$ . Unfortunately, due to the

**Table 4.** Expression of  $\rho v^2$  for the monoclinic phase. ( $Cp = \frac{C_{11}+C_{22}}{2}$ ,  $Cm = \frac{C_{11}-C_{22}}{2}$ ,  $C_{66}^* = C_{66} + C_{16} + C_{26}$ , and  $C_{16}^* = C_{16} - C_{26}$ ).

Direction/mode	Monoclinic phase
[100] $L$	$\gamma_1 \rightarrow \frac{1}{2}(C_{11} + C_{66} + \sqrt{(C_{11} - C_{66})^2 + 4C_{16}^2})$
$T_{[010]}$	$\gamma_2 \rightarrow \frac{1}{2}(C_{11} + C_{66} - \sqrt{(C_{11} - C_{66})^2 + 4C_{16}^2})$
$T_{[001]}$	$\gamma_3 \rightarrow C_{55}$
[010] $L$	$\gamma_4 \rightarrow \frac{1}{2}(C_{22} + C_{66} + \sqrt{(C_{22} - C_{66})^2 + 4C_{26}^2})$
$T_{[100]}$	$\gamma_5 \rightarrow \frac{1}{2}(C_{22} + C_{66} - \sqrt{(C_{22} - C_{66})^2 + 4C_{26}^2})$
$T_{[001]}$	$\gamma_6 \rightarrow C_{44}$
[001] $L$	$\gamma_7 \rightarrow C_{33}$
$T_{[100]}$	$\gamma_8 \rightarrow \frac{1}{2}(C_{44} + C_{55} + \sqrt{(C_{44} - C_{55})^2 + 4C_{45}^2})$
$T_{[010]}$	$\gamma_9 \rightarrow \frac{1}{2}(C_{44} + C_{55} - \sqrt{(C_{44} - C_{55})^2 + 4C_{45}^2})$
[110] $L$	$\gamma_{10} \rightarrow \frac{1}{2}(Cp + C_{66}^* + \sqrt{(C_{12} + C_{66}^*)^2 + (Cm + C_{16}^*)^2})$
$T_{[1\bar{1}0]}$	$\gamma_{11} \rightarrow \frac{1}{2}(Cp + C_{66}^* - \sqrt{(C_{12} + C_{66}^*)^2 + (Cm + C_{16}^*)^2})$
$T_{[001]}$	$\gamma_{12} \rightarrow \frac{C_{44}+C_{55}+2C_{45}}{2}$

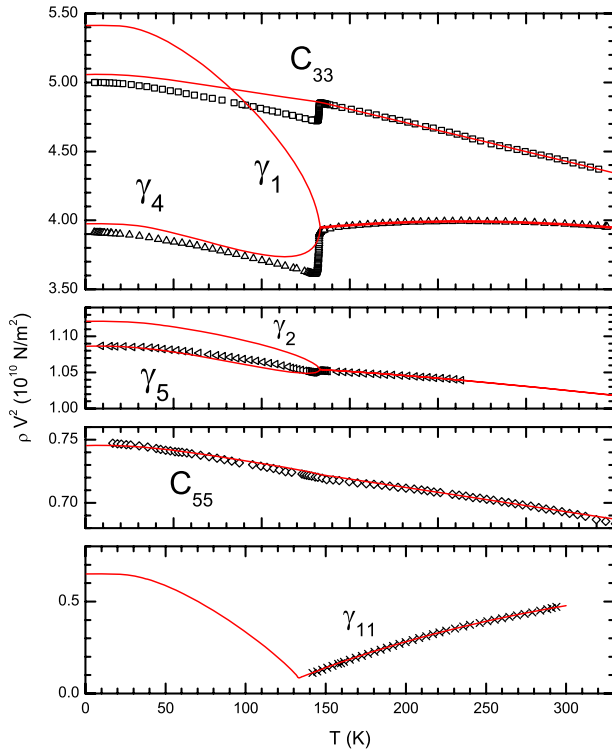


**Figure 5.** Temperature dependence of  $\rho v^2$  measured along the principal crystallographic directions of  $\text{Rb}_4\text{LiH}_3(\text{SO}_4)_4$ . The experimental results are represented by open symbols while the continuous lines correspond to predictions derived from the pseudo-proper ferroelastic model.

large acoustic attenuation, we were unable to obtain data in the ferroelastic phase or even close to the critical point. Significant decreases at the critical point are also observed in the value of  $\gamma_1$  (longitudinal modes propagating along [100]) and  $C_{33}$ , approximately 8% and 2.5%, respectively. Finally, anomalies on the other modes are visible, however, with much smaller variation. In general, we note that the temperature/pressure dependence in the paraelastic phase is

**Table 5.** Parameters for the anharmonic contribution.

	$\Theta_i$ (K)	$\alpha_{Ti}$	$\alpha_{Pi}$ (GPa $^{-1}$ )
1	95	0.044	0.167
3	95	0.058	0.187
4	95	0.028	0.040

remarkably well captured by the pseudo-proper ferroelastic model. However, below the critical point, a clear departure is observed for  $\gamma_1$  and  $C_{33}$ . We attribute those differences to the existence of structural domains in the low temperature ferroelastic phase. In the case of  $\text{Rb}_4\text{LiH}_3(\text{SO}_4)_4$ , these domains have been effectively observed and they consist of two mutually perpendicular walls inclined at 35° relative to the  $x$ -axis [8].

## 6. Soft acoustic mode

In their initial work, Mróz *et al* [9] claimed that  $\text{Rb}_4\text{LiH}_3(\text{SO}_4)_4$  could be described as a proper ferroelastic compounds and that the acoustic mode associated with the order parameter  $e_s$  showed incomplete softening at  $T_c$ . As typical proper or pseudo-proper ferroelastic compounds [12, 13] show complete softening, it is thus imperative to re-examine that claim. In order to determine the effective modulus of the soft mode, we first need to identify the elastic submatrix related to the strain components  $e_1 - e_2$  and  $e_6$ . For a  $4 \rightarrow 2$  ferroelastic phase transition this corresponds to

$$\begin{pmatrix} \frac{C_{11}-C_{12}}{2} & C_{16} \\ C_{16} & C_{66} \end{pmatrix} \quad (19)$$

which is different from the matrix used by Mróz *et al* [9]. Considering that elastic tensors are necessarily symmetric, it is clear that the form used by Mróz *et al* [9] is incorrect, as well as all the non-symmetry ferroelastic submatrices listed by Boccara [27]. Thus, the correct expression for the soft modulus, obtained by finding the eigenvalues of the submatrix

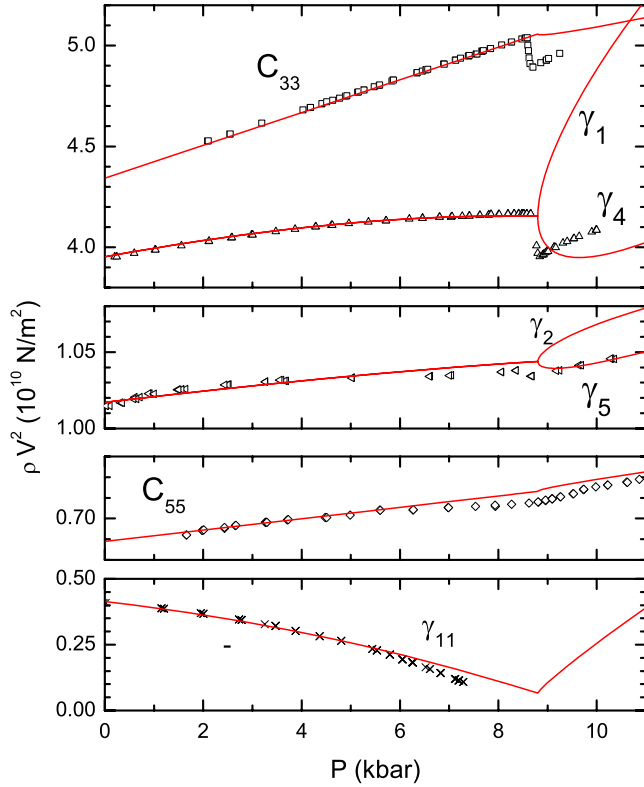


**Figure 6.** Pressure dependence of  $\rho v^2$  measured at room temperature along the principal crystallographic directions of  $\text{Rb}_4\text{LiH}_3(\text{SO}_4)_4$ . The experimental results are represented by open symbols while the continuous lines correspond to predictions derived from the pseudo-proper ferroelastic model.

equation (19), corresponds to

$$C_s = \frac{1}{2} \left( \frac{C_{11} - C_{12}}{2} + C_{66} - \sqrt{\left( \frac{C_{11} - C_{12}}{2} - C_{66} \right)^2 + 4C_{16}^2} \right) \quad (20)$$

while the direction of propagation [23] is given by

$$\tan 4\varphi = \frac{4C_{16}}{C_{11} - C_{12} - 2C_{66}}. \quad (21)$$

Using values of elastic constants at room temperature, the direction for complete softening in  $\text{Rb}_4\text{LiH}_3(\text{SO}_4)_4$  should correspond to  $\varphi \cong 12^\circ$  relative to the [110]. As that direction does not coincide with one of the principal crystallographic directions, this has contributed to delaying the experimental determination of the actual soft mode. In figure 7 we present new ultrasonic data that illustrate the temperature dependence of the elastic modulus for transverse waves propagating and polarized in the  $xy$ -plane. The direction of propagation is identified by an angle  $\phi$  measured away from the  $x$ -axis. Moreover, as no ultrasonic signal was detected in the ferroelastic phase, due to a rapid increase in the acoustic attenuation, our results are combined with Brillouin scattering data [9]. Figure 7 shows an increase in softening as the direction of propagation is changed from  $\phi = +54^\circ$  to  $35^\circ$ . The experimental results are compared to predictions

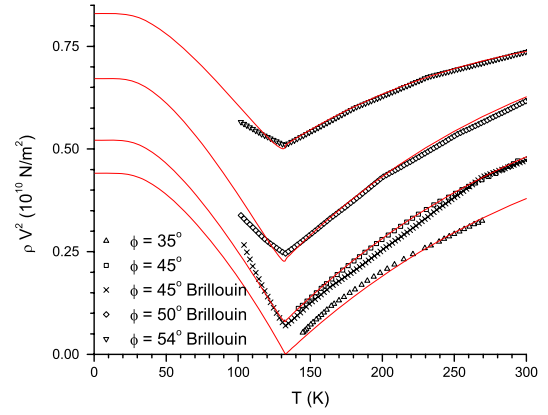


**Figure 7.** Temperature dependence of  $\rho v^2$  for transverse waves polarized in the  $xy$ -plane and propagating at an angle  $\phi$  relative to the  $x$ -direction. The experimental data, from ultrasonic (this work) and Brillouin [9] scattering measurements, are represented by symbols while continuous lines represent predictions obtained from the pseudo-proper ferroelastic model.

derived from the pseudo-proper model (continuous lines) which captures the overall temperature dependence. Finally, considering that the pseudo-proper model indicates complete softening at  $T_c$ , and that the experimental data agree well with those predictions, we conclude that there is no experimental evidence that  $\text{Rb}_4\text{LiH}_3(\text{SO}_4)_4$  shows incomplete softening  $T_c$ .

## 7. Conclusions

In this investigation, we present a detailed analysis of the elastic properties of  $\text{Rb}_4\text{LiH}_3(\text{SO}_4)_4$ . A substantial set of experimental data, as a function of temperature and pressure, is compared to a Landau model associated with a  $4 \rightarrow 2$  pseudo-proper ferroelastic phase transition. The model assumes that the elastic anomalies are due to the coupling with a B optical mode which acts as the principal order parameter. The proposed model is tested using a minimum number of coupling parameters, adjusted using the temperature dependence of the Raman soft B mode at  $31 \text{ cm}^{-1}$  [16], the thermal expansion data [8], and the pressure dependence of the critical temperature  $dT_c/dP = 19.1 \pm 0.2 \text{ K kbar}^{-1}$  (determined in this work). Our analysis shows that within the framework of the pseudo-proper ferroelastic model, it is possible to obtain predictions that account for the temperature/pressure dependence of all elastic constants. No such quantitative agreement is achieved using a proper ferroelastic model. Departure from the pseudo-proper model's predictions, principally on  $C_{33}$  and  $\gamma_1$ , is attributed to structural domains emerging in the ferroelastic phase. Thus, as argued in this investigation,  $\text{Rb}_4\text{LiH}_3(\text{SO}_4)_4$  presents all the characteristics associated with a pseudo-proper ferroelastic transition. We also demonstrate that there is no experimental evidence of incomplete softening at  $T_c$ . In fact, the elastic properties of  $\text{Rb}_4\text{LiH}_3(\text{SO}_4)_4$  are very similar to those of  $\text{BiVO}_4$  which shows a  $4/m \rightarrow 2/m$  pseudo-proper ferroelastic transition. Raman measurements [12] on  $\text{BiVO}_4$  show clear evidence of softening of the optical  $B_g/A_g$  mode. As for

$\text{Rb}_4\text{LiH}_3(\text{SO}_4)_4$ , the direction of propagation for the soft acoustic transverse mode is a few degrees away from [110] ( $\phi_0 = 10^\circ$ ). Moreover, in their analysis, Tokumoto *et al* [28] show that the temperature dependence of the soft mode is nonlinear and that complete softening is reached at  $T_c$ . These similarities are not accidental as both compounds belong to the same irreducible representation. The elastic properties of  $\text{BiVO}_4$  have been analyzed by David [21] and their predictions are similar to those presented in this work. In conclusion, the ferroelastic character of  $\text{Rb}_4\text{LiH}_3(\text{SO}_4)_4$  is not unique and should also be compared with that of  $(\text{NH}_4)_4\text{LiH}_3(\text{SO}_4)_4$  [29].

## Acknowledgments

This work was supported by grants from the Natural Science and Engineering Research Council of Canada (NSERC), Canada Foundation for Innovation (CFI) as well as by the Ministry of Science and Higher Education (Poland), grant No. 1 PO3B 066 30.

## References

- [1] Mróz B, Kiefte H and Clouter M J 1988 *Ferroelectrics* **82** 105
- [2] Mróz B, Tuszyński J A, Kiefte H and Clouter M J 1989 *J. Phys.: Condens. Matter* **1** 4425
- [3] Wolejko T, Piskunowicz P, Breczewski T and Krajewski T 1988 *Ferroelectrics* **81** 175
- [4] Wolejko T, Pakulski G and Tylczynski Z 1988 *Ferroelectrics* **81** 179
- [5] Piskunowicz P, Breczewski T and Wolejko T 1989 *Phys. Status Solidi a* **114** 505
- [6] Minge J and Krajewski T 1988 *Phys. Status Solidi a* **109** 193
- [7] Pietraszko A and Lukaszewicz K 1988 *Z. Kristallogr.* **185** 564
- [8] Mróz B, Kim S M, Powell B M, Kiefte H and Donabarger R L 1997 *Phys. Rev. B* **55** 11174
- [9] Mróz B, Kiefte H, Clouter M J and Tuszyński J A 1991 *J. Phys.: Condens. Matter* **3** 5673
- [10] Breczewski T, Gomez-Cuevas A, Perez-Mato J M and Bocanegra E H 1990 *Solid State Commun.* **76** 639
- [11] Peercy P S and Fritz I J 1974 *Phys. Rev. Lett.* **32** 466
- [12] Pinczuk A, Burns G and Dacol F H 1977 *Solid State Commun.* **24** 163
- [13] Hellwig H, Goncharov A F, Gregoryanz E, Mao H and Hemley R J 2003 *Phys. Rev. B* **67** 174110
- [14] Carpenter M A and Salje E K H 1998 *Eur. J. Mineral.* **10** 693
- [15] Salje E K H 1990 *Phase Transition in Ferroelastic and Co-Elastic Crystals* (Cambridge: Cambridge University Press)
- [16] Aktas O, Clouter M J and Quirion G 2009 *J. Phys.: Condens. Matter* **21** 285901
- [17] Witting J, Eichler A and Angew Z 1968 *Physica* **25** 319
- [18] Tolédano P, Fejer M M and Auld B A 1983 *Phys. Rev. B* **27** 5717
- [19] Errandonea G and Savary H 1981 *Phys. Rev. B* **24** 1292
- [20] Tinkhan M 2003 *Group Theory and Quantum Mechanics* (New York: Dover)
- [21] David W I F 1983 *J. Phys. C: Solid State Phys.* **16** 5093
- [22] Salje E K H 1991 *Acta Crystallogr. A* **47** 453
- [23] Dieulesaint E and Royer D 1980 *Elastic Waves in Solids* (New York: Wiley)
- [24] Rehwald W 1973 *Adv. Phys.* **22** 721
- [25] Varshni Y P 1970 *Phys. Rev. B* **2** 3952
- [26] Quirion G, Kelly A, Newbury S, Razavi F S and Garrett J D 2003 *Can. J. Phys.* **81** 797
- [27] Boccara N 1968 *Ann. Phys.* **47** 40
- [28] Tokumoto H and Unoki H 1983 *Phys. Rev. B* **27** 3748
- [29] Mróz B, Kiefte H, Clouter M J and Tuszyński J A 1993 *J. Phys.: Condens. Matter* **5** 6377